

Carbon nanotubes for organic/inorganic hybrid solar cells

Elif Arici¹⁺ and Smagul Karazhanov²

¹Energie Institute, Istanbul Technical University, Ayazağa Kampüsü, 34469 Maslak – Istanbul, Turkey

²Department for Solar Energy, Institute for Energy Technology, Instituttveien 18, 2027 Kjeller, Norway. E-mail: smagulk@ife.no, mobile: (+47) 9651 7797, Fax: (+47) 6389 9964

Abstract

This article describes the material properties and thin film forming strategies for carbon nanotubes. It summarizes the developments and the challenges related to doping and reviews the highlights over the past decade about organic/inorganic hybrid solar cells using carbon nanotubes (CNTs). Replacing the indium tin oxide electrode by CNT spiderwebs have displayed solar cell efficiencies of about 3-4 % for organic bulk heterojunction devices, enabling a cost effective fabrication of organic solar cells by roll-to-roll process. Investigations on SWNT/Si hybrid solar cells with efficiency of 17 % demonstrate the possibility of wide range applications of SWNTs in organic/inorganic hybrid solar cells.

Keywords: carbon nanotubes, hybrid solar cells, silicon, organic and inorganic solar cells, transparent and conducting films

¹ **Corresponding author: e-mail:** aricibogner@itu.edu.tr

1. Introduction

Transparent conducting films (TCF) exhibit transparency to the visible light and at the same time possess good electrical conductivity. Such films have found applications in many electrical devices such as solar cells, sensors, electrodes for displays of TVs, touch screens, etc [1, 2]. The most widely used TCF is the indium tin oxide (ITO). However, the material contains indium, which is a rare metal typically found in limited geographical locations. Materials cost, importance of indium resources, and the demand in using ITO is soaring, so that in the near future ITO can become one of the strategic materials that cannot satisfy the increasing demand. These drawbacks have led to increasing the research attention to searching the indium-free TCF. Recently, graphene [3-6] and CNTs (CNT) [7, 8] have emerged as promising In-free candidates to be used as transparent and conducting materials [9]. Studies and applications of graphene as a TCF in photovoltaic technology [10-14], e.g. in Si based solar cells [15-18], are in an early phase. Considering the short history of graphene, several fundamental questions are yet to be answered in relation to its preparation and implementation in devices. CNTs might be also good candidate for replacement of ITOs. This issue specially is important in organic solar cells, enabling to form highly flexibel solar cells by roll-to-roll processing.

In the past few years, the role of CNTs in solar cells has been extended from the effective hole transporting materials for organic solar cells to photo active materials for Si-based cells. Hybrid solar cells were fabricated by depositing intrinsic *p*-type SWNT thin-films on *n*-type Si wafers without involving any high-temperature process for *p-n* junction formation. The hybrid solar cells showed a high power-conversion-efficiency of 17% [19]. These results together with the advanced properties of CNTs such as low reflectance, high mechanical stability and chemical resistance to air are the strong motivations for the further development of this topic. Optimizing chemical properties of CNTs could also serve as a

platform for next-generation solar cells such as, e.g., hybrid CNT/classical inorganic (CIGS, CdTe etc.), CNT/polymer, and all carbon solar cells.

This review will focus on developments and challenges related to CNTs and on highlights over the past decade about its applications in organic and hybrid solar cells. At first, some basic information on different types of CNT structures, their opto-electronic properties and characterization tools will be briefly addressed. CNTs synthesized and purified using different methods have diverse physical and chemical properties, which will yield films with distinct performance. Therefore, the chemical methods of preparation of CNTs for photovoltaic applications will be analyzed in Sec. 2. One of the major advantages in using CNTs is their ability to be deposited to substrates from solution. One of the primary research areas for making transparent conductive films is to process the CNT material into printable inks. The Sec. 3 will outline major approaches to disperse CNTs and focus on the most important details with regards to processing CNT thin films from solution. In Sec. 4.1, a variety of doping techniques for making transparent conductive CNT films will be presented and the post-treatment effects will be evaluated. The latest progress on CNT transparent conductive films and their applications in organic bulk heterojunction solar cells using a P3HT/PCBM blends will be summarized in Sec 4.2. In Section 4.3, the role of CNTs in the photo active layer is briefly discussed and very recent developments on *p*-CNT/*n*-Si hybrid solar cells are summarized.

2. CNT structures and opto/electronic properties

CNTs are cylinder-shaped molecules with large aspect ratios. Radius of a CNT can be as small as a few nanometers. The length of CNTs can be in the range from 100 nm to 20 cm depending on the synthesis conditions. The walls of the tubes are made up of a hexagonal

lattice of carbon atoms analogous to the atomic planes of graphite. At their ends, they are capped by one half of a fullerene-like molecule. It is well known that the properties of CNTs are related to their structures. In the most general case, a CNT is composed of a concentric arrangement of many cylinders. Diameter of such multi-walled nanotubes (MWNTs) can reach up to 100 nm. Single-walled nanotubes (SWNTs) possess the simplest geometry and have been observed with diameters ranging from 0.4 nm to 3.0 nm. The formation of a SWNT can be visualized through the rolling of a graphene sheet.

MWNTs behave independent of their structural parameters as a metal, whereas the electrical characteristics of SWNTs depends on its chirality. The structural characterization of SWNTs is based on the orientation of the tube axis with respect to the hexagonal lattice given by its chiral vector, which is denoted by its chiral indices (n and m). SWNTs with chiral indices $n-m= 3j$ for $j=0$ are metallic (m -SWNTs) and all the others have non-zero band gap. SWNTs with $n-m = 3j$ for $j >0$ have a very small band gap of $E_g < kT$ referred to as “semi metals” and SWNTs with $n-m = 3j \pm 1$ (with $j >0$) have larger band gap (around 1eV) referred to as “semiconducting” SWNTs (s -SWNTs). Here k is the Boltzman constant and T is the temperature. Semiconducting behaviour of the SWNTs can be inverted to metallic behaviour by chemical doping as discussed in Sec 3.

A disadvantage of SWNTs is that the synthesis in most cases results in a mixture of the metallic and semiconducting SWNTs. Therefore, developing the strategies to separate metallic and semiconducting SWNTs is an actual target with great importance for solar cell applications of CNTs. Absorbance [20] and Raman [21] measurements are the characterization tools, which allows to distinguish whether the SWNT is a metallic or semiconducting. If the SWNTs are in the mixed state consisting of metallic and the semiconducting types, the samples possess the black color [22], because the absorption bands caused by the metallic and the semiconducting nanotubes cover almost the entire range of the

visible region. Absorbance spectra of SWNTs will be shifted to higher energies with decreasing the nanotube diameter [23]. Non-functionalized SWNTs shows photovoltaic response [24, 25]. The general consensus in the literature is that photocurrent generation is caused by electronic transitions between van Hove singularities in SWNTs which upon illumination leads to creation of excitons [26, 27].

Raman spectroscopy has been a very powerful tool to study electronic and vibrational properties as well as to analyse purity of CNTs [28, 29]. The two important Raman modes for SWNTs are the radial breathing mode (RBM) appearing at low frequencies and the tangential (*G* band) multi-feature coming up at higher frequencies. The disorder-induced (*D*) band gives information about the amount of amorphous carbon and related impurities. Raman spectra of MWNTs is similar to those of SWNTs. The primary differences are the lack of RBM modes and a much more prominent *D* band in MWNTs [30]. The more prominent *D* band in MWNTs is to be expected to a certain extent given by the multilayer configuration and indicates more disorder in the structure. The RBM features correspond to the coherent vibration of the C atoms in the radial direction, as if the tube were “breathing”. These features are unique for SWNTs and occur with frequencies ω_{RBM} between 120 and 350 cm^{-1} . The location of the RBM peak depends on the nanotube diameter ($0.7 \text{ nm} < d < 2 \text{ nm}$) following the rule $\omega_{\text{RBM}} \sim 1/d$. The *G*-bands are associated with sp^2 bonding in carbon systems and occur at frequencies between 1500 cm^{-1} - 1650 cm^{-1} . The central frequency of the *G*-band can be used for estimation of diameter of SWNTs. Furthermore, it allows to distinguish the metallic and semiconducting SWNTs each from other. The strong differences in *G*-band between the metallic and semiconducting SWNTs can be detected by in Raman measurements.

Like the other sp^2 -hybridized carbons, SWNTs also display *D*-band at 1250-1450 cm^{-1} . The intensity and shape of the *D*-band depends on concentration of carbon impurities and of surface defects. The *D*-band of the crude material with a peak at 1350 cm^{-1} is commonly quite

broad with a full-width-at-half-maximum (FWHM) at about $\sim 50 \text{ cm}^{-1}$. A sharp *D*-band with a FWHM at ~ 20 at 1350 cm^{-1} indicates to lower concentration of impurities and high crystallinity. On the other hand, if during purification acidic treatment will be used, then the *D* band can be broadened when side walls of the CNTs are partly oxidized.

3. Synthesis and purification strategies

CNTs can be synthesized from a variety of different materials and several catalysators will be used. Below we describe the three methods often used in synthesis of CNTs: electric arc-discharge, catalytic decomposition of gaseous hydrocarbons, and laser ablation. Electric arc-discharge technique uses two electrodes. At least one of the electrodes is made of graphite. Carbon atoms are generated through an electric arc discharge at $T > 3000^\circ\text{C}$ between the electrodes [31]. A large scale production of CNTs ($50 \text{ kg} \times \text{day}^{-1}$) can be achieved using this technique. The main advantage of the method is that the MWNTs can be obtained without any metal catalyst, while SWNTs are formed in the presence of suitable catalysts such as, e.g., Fe, Co, or Ni [32].

In laser ablation method of production of CNTs, an intense laser beam is used to vaporize the target consisting of admixture of graphite and metal catalyst in the flow of inert gas at temperatures $> 3000^\circ\text{C}$ [33]. A favor of this method is that the diameter of SWNTs can be controlled by reaction temperature [34]. Additionally, SWNTs produced by laser vaporization (LV) might have lower defect densities than tubes produced by chemical vapor deposition (CVD) [35].

Chemical vapor deposition (CVD) method involves decomposition of a gaseous hydrocarbon source (e.g., an alkane or CO) catalyzed by metal nanoparticles such as, e.g., Ni, Co or Fe. Particles are prepared by pyrolysis of suitable precursors (e.g., $\text{Fe}(\text{CO})_5$) at low

temperature in range 300-1200 °C. One of the drawbacks of the method is high defect density in the material owing to low synthesis temperature compared to arc discharge and laser ablation methods. Typical content of SWNT and MWNT obtained from the method is in the range 30-50 % and 30-99%, respectively [28, 32].

Isolated and relatively pure SWNTs can be directly synthesized by CVD on a solid substrate. In this case, the catalyst particles are deposited onto a substrate, and individual SWNTs of almost uniform diameters will be grown at elevated temperatures >600 °C from the catalyst particles, using for instance methane [36] or an alcohol vapor [37, 38] as the carbon source. An important technological aspect for a successful integration of CNTs in solar cells is related to the purification strategy. The typical by-products are fullerene, amorphous carbon and graphitic polyhedrons with enclosed metal particles [28]. Additionally, CNTs may contain defects formed during synthesis. Typically, 1-3% of the carbon atoms are located at a defect site [39].

A typical purification process consist of several steps:

1. Fullerenes can be removed in certain organic solvents, for example using Soxhlet extraction in toluene.
2. The amorphous carbon can be eliminated easily, because of high density of defects in it, which allow it to be oxidized at 350 °C in air or by sonification in H₂O₂.
3. After the removal of carbon species, the metal particles can be removed by heating in non-oxidizing acid solution (dilute HCl or dilute HNO₃) by subsequent filtering.
4. Polyhedral carbons having similar oxidation rates to SWNTs, are not easy to remove. Also, metal impurities encapsulated with carbon layers might make them unable to dissolve in acids. Surfactants are added into the acidic medium to disperse the CNT bundles surrounding metal impurities. Multi-step purification procedures for polyhedral carbons using selective surfactants are described in detail in Refs. [28, 32, 40].

Concerning the by-products, the size distribution of them may be very broad depending on the synthesis conditions. Therefore it is rather difficult to develop a purification method without creating defect sites. In most cases, a final annealing at temperatures 1000-2800 °C in vacuum is needed to reduce the defect sites.

After the synthesis using the above methods, usually one-third of the SWNTs will be metallic (*m*-SWNTs) whereas the rest two-thirds exhibit semiconducting properties (*s*-SWNTs). In order to achieve more accuracy in electronic properties, the semiconducting and metallic single walled CNTs must be separated. Some of the separation methods are briefly described below: since the mean diameter of CNTs controls the number of possible chiralities, it can be the prerequisite tool for obtaining SWNTs with homogeneous, i.e., either purely *p*-type semiconducting or metallic material properties, electrical properties. The studies show that size distribution of the catalyst particles also has much more significant impact on mean diameter of CNTs than the selected methods or the temperature [41-43]. It was found out that SWNTs synthesized with a diameter >2 nm have enhanced ratio metallic/semiconductor CNTs [44]. Recently, reducing the diameter of SWNT to >2 nm has been achieved in several reports (see, e.g., Refs. [23, 45, 46]) by changing the relative Co-Mo content in the bimetallic catalyst composition [23], by adding acetonitrile to ethanol carbon feedstock during synthesis [45], and by decoupling the catalyst formation and SWCNT growth processes [46] for a selective growth of semiconducting SWNTs using CVD.

Another idea was to use density gradient ultracentrifugation and agarose gel separation, a routine method for resolving DNA for the chemical separation of metallic and semiconducting CNTs. The surfactant sodium dodecyl sulfate plays the key role. This surfactant and its chemical derivatives have relatively low dispersibilities, which is likely due to their common structural feature, i.e. straight alkyl tails and charged head groups, and appeared to enable *m*- and *s*-SWCNTs to be distinguished. Using an agarose gel for

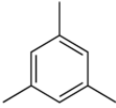
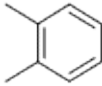
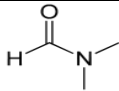
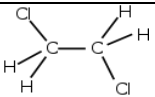
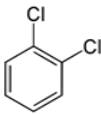
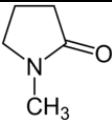
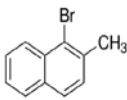
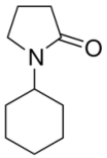
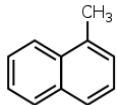
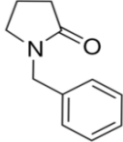
electrophoresis the *s*-SWCTs but not *m*-SWCTs are selectively absorbed to the gel [47]. For more detailed description of the methods see, e.g., the Refs. [47-52].

3. CNT dispersions and thin film formation

Most of the organic solvents are unable to disperse CNTs in large concentrations to be interesting for industrial applications (>0.1 mg/mL). Table I displays solubility of CNT at room temperature and surface tension of the organic solvents [53-56]. In general, the most effective method to identify solvents to disperse nanoparticles in solvents relies on matching the surface energy of the solvent to that of the nanoparticles. SWNTs have surface energies of about 70 mN/m [57]. For all solvents, the surface tension is about 30 mN/m below the surface energy [58] of the solids. This means that efficient solvents for SWNTs are the one with surface tensions of about 40 mN/m. But the expected relationship is not approved in practice. Because of their uniaxial growth, a strong tendency to form bundles occurs as a result of the strong van der Waals interaction between the tubes. Solvents with electron pair donation, higher polarity and low values of the hydrogen bond donation parameter, such as *N*-Methyl-2-pyrrolidinone (NMP), dimethyl formamide (DMF), dichloroethane (DCE) and cyclohexyl pyrrolidone have been identified as the best organic solvents to disperse CNTs to individually separated nanotube particles. Nanotubes in NMP spontaneously exfoliate on dilution of SWNT–NMP dispersions, leading to a dynamic equilibrium characterized by significant populations of pristine individual nanotubes and small bundles.

Earlier, it was demonstrated in Ref. [55] that cyclohexyl-pyrrolidone can disperse SWNTs up to 3.5 g/L with high levels of individual tubes or small bundles and can keep it stable for at least one month. A similar solvent 1-benzyl-2-pyrrolidinone (NBenP) with surface tensions of 45.0 mN/m has been reported also as a promising alternative. Their ability to disperse and exfoliate nanotubes might be reasoned due to the low energetic cost of

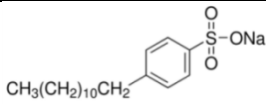
TABLE I. Solubility parameter of CNTs in organic solvents.

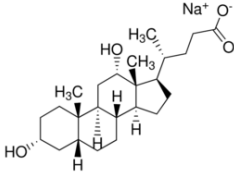
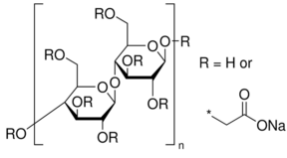
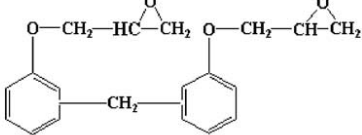
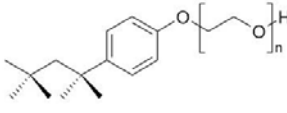
Solvent	Structure	g/l	Surface tension mN/m
1,3,5-Trimethylbenzene [53]		0.0023	28.80
1,2-Dimethylbenzene [53]		0.0047	30.10
Dimethylformamide [53]		0.0072	37.10
1,2-Dichloroethane [54]		0.0087	38.75
1,2-Dichlorobenzene [53]		0.095	38.75
N-Methyl-2-pyrrolidinone [53]		0.010	40.79
1-Bromo-2-methylnaphthalene [53]		0.023	41.38
1-Cyclohexyl-2-pyrrolidon [55]		3.5	43
1-Methylnaphthalene [53]		0.025	38.60
1-Benzyl-2-pyrrolidinone [56]		3.5	45.00

exfoliation in such solvents. Finally, because of un-toxicity, these solvents are more user-friendly than the traditional ones such as NMP or DMF. Disadvantage of these solvents is their high boiling point (B_p of about 150 °C) [53, 55].

Clearly, CNTs are also extremely hydrophobic [59]. But due to the experimental requirements, such as doping process in acidic media, the aqueous dispersion of CNTs have notable advantages for the preparation of transparent electrodes. Surface modification by covalently functionalizing the CNT walls using aryl-carboxylic acid or aryl-hydroxyl groups [60] was a successful strategy to enhance the nanotube dispersion in water. Other dispersion methods include covalent modification of the surface via acid purification [61], thermally activated coordination chemistry and/or photochemical functionalization [62]. But all these methods create groups at CNT walls, which can act as recombination. Alternatively, CNTs are suspended in *aqueous media* by non-covalent interactions using surfactants [7, 20, 63-65]. These materials exfoliate nanotubes very efficiently and can disperse nanotubes at reasonably high concentrations. The chemical structures of mostly used surfactants for electrode preparation and the preferred thin film fabrication methods are listed in Table II. The detailed description of the thin film preparation method is available in corresponding references.

TABLE II. *Surfactants used for the thin film formation of SWNTs in aqueous solutions.*

Surfactant	Structure	Method
Sodium dodecylbenzenesulfonate (SDBS) [66]		Spray coating/ Acid treatment
Sodium dodecyl sulphate (SDS) [66]	$\text{NaC}_{12}\text{H}_{25}\text{SO}_4$	Spray coating/ Acid treatment

<p>Sodium deoxycholate (DOC) [66]</p>		<p>Drop casting/ Acid treatment</p>
<p>Sodium carboxymethyl cellulose (CMC) average $M_w \sim 70,000$, powder [7]</p>		<p>Spray coating/ Acetone treatment</p>
<p>Epoxy resin (Epon 862/EPI Cure W system [65]</p>		<p>Filter method using porous alumina matrix/Annealing</p>
<p>Octyl-phenol-ethoxylate (Triton X-100) [65]</p>		<p>Spin casting</p>

SWNTs thin film morphologies can be modulated by using CNT dispersions in different surfactant/solvent mixtures for spin-casting, because the bundle thickness of the SWNTs depends on the strength of surfactant/CNT interaction. The effect on SWNT morphology by using three different surfactants; deoxycholate (DOC), sodium dodecylbenzenesulfonate (SDBS) and sodium dodecylsulphate (SDS) are studied by atomic force microscopy. SDBS has a weak adhesion on CNT walls in comparison to DOC. Therefore, the strong van der Waals interaction between the CNTs leads to thick bundle-like CNT aggregates using SDBS. Upon using the DOC as surfactant, the interaction between the CNT and the surfactant is more stronger than van der Waals interaction between CNTs. Then the bundle formation of SWNTs can be suppressed leading to a more interconnected network of SWNTs. To understand the difference in the network morphology for the different surfactants, it is important to consider the film formation process, which has two critical steps: concentration of the dropped solution by drying during the thin film coating and replacement

of the surfactant after film formation. The dispersion ability varies as $\text{DOC} > \text{SDBS} > \text{SDS}$, and thus, the attractive force between the SWCNTs is believed to change as $\text{SDS} > \text{SDBS} > \text{DOC}$. DOC dispersion presents the case of a weak attractive force between CNTs. In this case, an individual random network can be formed being maintained in the dispersion. For the films formed from DOC, fine mesh structures were observed. The thicknesses of the bundles were approximately 1 nm for DOC, respectively.

When the attractive force between CNTs increases as in SDBS dispersion, the CNTs begin to align locally in the same direction. Long, bundled ropes formed a homogeneous and continuous but coarse mesh (approximately 10 μm). For the largest attractive force, such as the SDS dispersion, the CNTs form the thickest bundles [Fig. 1b]. A surfactant with a stronger dispersion ability should be in principle better suited to produce CNT electrodes, because it is important to keep the bundles thin to obtain highly transparent electrodes. On the other hand, the surfactant molecules with lower dispersion abilities could adhere not so strongly that the presence of residual surfactant on the CNTs after washing is negligible, leading to low contact resistances.

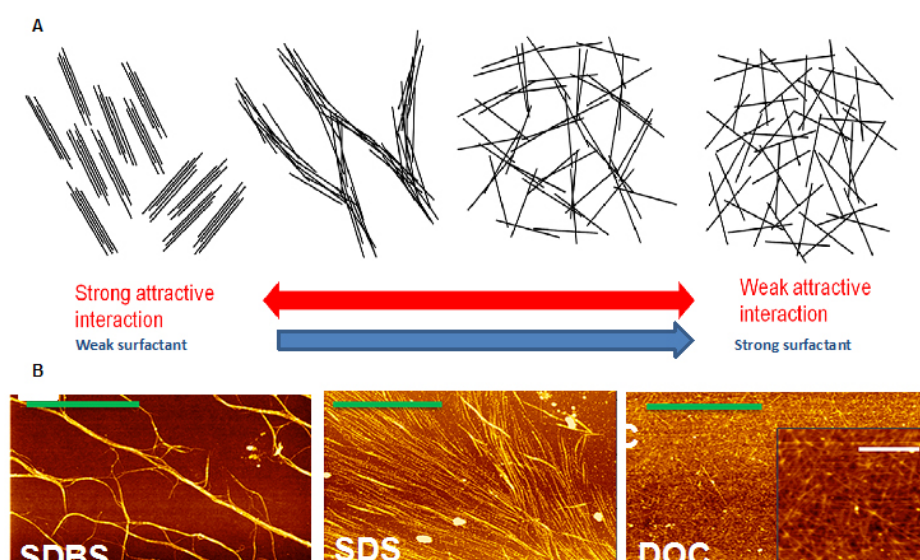


Figure 1. a) Schematic images of the CNTs with different strength of attractive interactions in solution. b) AFM images of drop casted SWNT layers using SDBS, SDS and DOC as surfactant (From Ref. [66]).

According to conductivity measurements, SDS is the most favorable surfactant in this run. A sheet resistance of 57 Ω/sq at 65% transmittance of SWNT thin films have been obtained in Ref. [63] with electrical conductivity in excess of $6700 \text{ S}\cdot\text{cm}^{-1}$. The sheet resistance is of the same order with that of surfactant-free films [63]. Using the SDS containing CNT inks, smooth electrodes can be prepared by using the spin-coating and also spray coating techniques. Adding the surfactant into the mixture of CNT in aqueous media often requires processes, such as high-power ultrasonication, which may degrade the nanotube surface and may reduce the average lengths of the tubes.

The filter/transfer (FT) approach has the benefit of yielding loosely bundled films that permit easy removal of insulating surfactants by washing in deionized water. This method involves vacuum filtering of a dilute suspension of nanotubes in aqueous solution over a porous alumina filtration membrane. The density of these films can be controlled by volume of the suspension [66]. By subsequent drying, the SWNT films can be lifted off with a polydimethylsiloxane (PDMS) stamp and transferred to a flexible poly-ethylene terephthalate (PET) substrate by printing. The printing method produces a relatively smooth, homogeneous film with a transmittance of 85% at 550 nm and a sheet resistance R_s of 200 Ω/sq after acid treatment [65].

Another method of synthesis of CNT electrodes is vertical growth on an transparent electrode. The advantages of this method is that the vertically grown CNT films exhibit high levels of structural perfection, long average tube lengths, high purity, and relative absence of tube bundles compared to those derived from the techniques described above. Using plasma

enhanced chemical vapor deposition (PECVD) method, critical properties of the tubes, such as diameter distributions and, possibly, chiralities, can be influenced by the size and composition of the catalyst [41, 67-69]. Growth temperature, pressure, and time can also affect properties, such as average tube length [70]. Aligned and patterned CNTs on silica (SiO_2) substrates have been synthesized by CVD using various precursors such as a mixture of ammonia/ethylene, ethylene/ hydrogen or only methanol at temperatures 750 °C - 600 °C [71-73]. After the growth, the CNTs were embedded in a dilute polymer or epoxy-composition by drop casting and could be easily peeled off from the substrate. The CNT/polymer blends can be diluted in deionized water to prepare highly concentrated three dimensional CNT networks using spin-cast technique.

For the application of vertically oriented CNTs as electrodes for organic solar cells, a direct growth of CNTs on a transparent substrate such as fluorine doped tin oxide might be profitable. Such studies revealed the challenge such as fluorine diffusion from the transparent oxide from the process gases at elevated temperatures, which has led to dramatic losses of electrical conductivity of the substrate. After exposure to CNT growth conditions, the samples were no longer transparent. They became rather translucent, indicating strong scattering of the light. The reason for these changes may be due to the reduction of SnO_2 to metallic tin, which forms isolated islands. Upon exposure to air, an isolating SnO_x layer is formed [74].

There are few studies (see, e.g., Ref. [75]) using ITO as the substrate for the vertically growth of CNTs. Growth of CNTs at temperatures around 500°C and at pressures ~20 mbar on ITO has been reported [75] using PECVD. This system resembles as a parallel plate radio frequency (RF) at 13.56 MHz capacitively coupled plasma (CCP) with C_2H_2 as carbon source, H_2/Ar as dilution medium and a heatable stage acting both as counter electrode and substrate holder [74]. Low cost substrates including aluminium and stainless steel can also be used for the vertical CNT growth when the electrode is used as back electrode in solar cell design [75].

4. CNTs for photovoltaics

The dominant transparent conductive material used for photovoltaic applications today is ITO with a demand growing at 20 % per annum. It has been studied and refined over the years and may therefore offer many advantages [74, 76]. However, ITO tend to fracture by deformations, so, they are not really suitable for using in flexible solar cells. In case of organic photovoltaics, absence of high performance flexible electrodes that can be processed at plastic compatible temperatures $<150\text{ }^{\circ}\text{C}$, limits commercialisation of roll-to-roll processed flexible large area solar cells. In addition, indium is a scarce and expensive element. All these arguments can hurdle the large-scale and low cost OPV production, therefore an intense research is devoted to the development of alternative transparent electrodes for OPVs.

Analysis showed that the work function for metallic CNTs 4.5-5.1 eV is approximately the same as that of ITO 4.4-4.9 eV [77]. Furthermore, CNT possess the other technologically interesting properties as the excellent conductivity, good transparency in the visible and near infrared regime, wettability on different surfaces using additives and surface modification, high thermal stability and mechanically robustness. As the synthesis methods and CNT thin film morphology are the critical factors for the expansion of the full potential of the material properties listed above, the reported physical properties of CNT films are very much dependent on the thin film preparation and the post-treatment effects.

4.1 Doping strategies for CNT thin layers

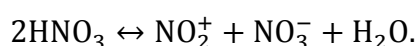
Taking the advantage of high aspect ratio to form a percolation network at low concentrations (0.01 wt %), CNTs were first used as electrically conductive fillers in plastics. Disordered CNT-polymer composites reach electrical conductivities as high as $100\text{ S}\times\text{cm}^{-1}$ at

10 wt % loading [78]. SWNTs as well as MWNTs are investigated also as electrodes for solar cells. The general opinion is that in the applications as electrodes in solar cells performance of SWNTs is better than that of MWNTs. The enhanced transparency of the thin films together with the low density of defects at the surface are the arguments behind the advanced material property. In this section, we discuss doping of SWNTs to create metallic thin layers as well as the doping-induced stability of the films. In a single CNT, isolated from the CNT bundle, since carriers in their electronic structure are weakly bound to phonons, CNTs show a “ballistic” charge transport along the main nanotube axis with charge carrier mobilities up to $10000 \text{ cm}^2\text{Vs}^{-1}$ [79]. However, electrical conductivity of CNT thin films are affected by many factors such as the length of the nanotubes, the surface defect density and the junction resistance between the nanotubes.

The basic material development strategy for enhancing the electrical conductivity of CNT thin films is to develop new synthesis routes for selective and defect free CNT production. Additionally, the junction resistance between the nanotubes is directly related to the morphology affected by the degree of CNT dispersion in solution (bundle thickness), thin film preparation methods and parameters as well as the aspect ratio of the CNTs. Reports have shown [80] that transparent SWNT films of 87% transmittance at 550 nm can be produced with sheet resistance of $100\text{-}160 \text{ }\Omega/\text{m}^2$ without any post-treatment steps. Values in these ranges are still higher than those of ITO films having sheet resistances as low as 10 and $60 \text{ }\Omega/\text{m}^2$.

In this section, we want to discuss the influence of doping through chemical treatment to enhance the bulk conductivity of SWNT thin films. Significant doping can result in the metallization of semiconducting carbon tubes through the effective pinning of the Fermi level inside either the conduction or valence band with electron or hole doping, respectively. Generally, X-ray photoemission spectroscopy (XPS) is used to get insight into the influence

of doping effects on SWNT films. Given by the typical feature of one-dimensional crystals, the density of the states (DOS) for SWNTs is not a continuous function of energy, but it increases in a discontinuous spike (Van Hove singularities). The first van Hove peaks in semiconducting SWNTs lie about 0.26–0.8 eV below the Fermi level, and the second peak is at about 0.5–1.5 eV below the Fermi level [81]. For comparison, there is just one characteristic van Hove transition in metallic tubes, located at less than 1 eV below the Fermi level [82]. Chemical way of tuning the Fermi level by doping can increase the electrical conductivity of the SWNTs while decreasing the intertube resistance. For developing transparent anodes *p*-doping of the SWNT films is preferred by using strong acids and inorganic solvents such as HNO₃, H₂O₂, SOCl₂, FeCl₃, AuCl₃. Doped films using HNO₃ and SOCl₂ were found to possess twice larger electrical conductivity with sheet resistance as low as 140–170 Ω/cm² with an optical transmittance above 80% at 550 nm. Using both dopands the sheet resistance was reduced to 115 Ω/cm² [83]. As a strong acid, HNO₃ can be intercalated reversibly into the expanded lattice of the SWNT bundles after undergoing an autoprotolysis reaction:



It is assumed that the oxidizing reagent NO₃⁻ forms stable planar resonating electronic structure originated from *sp*² hybridization. The hypothesis, supported by transmission spectroscopy analysis, is that after the HNO₃ purification process, the salts of the form (SWNTⁿ⁺)(NO₃⁻)(HNO₃)_m were formed. Also the *G*-band of Raman spectra can be used to probe charge transfer from doping, to distinguish the metallic and semiconducting SWNTs through their strong changes in line shapes.

An important question hereby is the stability of the doping effect. Many studies present reversibility of the doping effect under different conditions such as humidity, thermal stress and chemical aging. The possible reasons for the doping instability are the enhanced

chemical reactivity and the desorption of dopants out of the films. Desorption of the dopants out of the film creates mobile ions in the network, which can damage the device fabricated on the top of the films. Charge transfer doping effects using HNO_3 have been shown to be easily reversible with time and also reversible with annealing at moderate temperatures (30-70 °C), especially by dipping the SWNT thin layer in HNO_3 solution [84]. Usage of HNO_3 vapor instead of liquid [85] has led to enhancement of stability of the doped SWNT layers. Recently, extended testing in open air at room temperature using the protecting layer of poly(3,4-ethylenedioxythiophene)-poly(styrenesulfonate) aqueous solution (PEDOT:PSS, Baytron) on the top of the SWCNT layer has shown the stable sheet resistances with aging period of 1500 h. PEDOT:PSS layer may prevent the reaction of acryl chloride groups on the nanotube surface with air and prevent desorption of HNO_3 at 80 °C [83].

In 2013, a great promise for the improvement of the organic solar cell parameter were reported using gold (III) chloride hydrate in nitromethane after the HNO_3 treatment of CNT electrodes. AuCl_3 doped CNT films have sheet conductances about 66% of their original doped value after 50 days and sheet conductances about 20% of their original doped value after heating to 200 °C [86]. A strong and stable doping of CNTs has been demonstrated [87] using MoO_x thin layers with a thickness less than 10 nm. Thermally annealed MoO_x -CNT composites form durable thin film electrodes with sheet resistances of 100 Ω/sq at 85% transmittance [87]. MoO_x films of identical thickness on glass have very high sheet resistances of the order of 300 Ω/sq and displayed no changes before and after annealing. In contrast, as deposited on the top of the CNT network, the presence of MoO_x already decreases the sheet resistance of CNT layer by a factor of ~2.

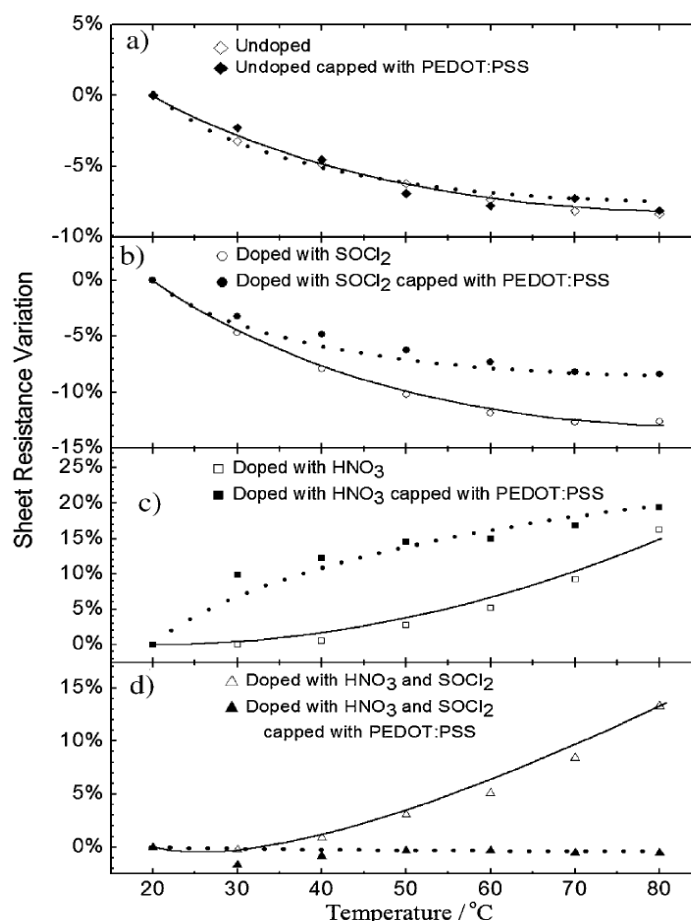


Figure 2. (From Ref. [83]) Sheet resistance increase of SWNT films versus temperature for (a) undoped films with and without a PEDOT:PSS layer, (b) for HNO₃ doped films with and without a PEDOT:PSS layer, and (c), (d) for HNO₃ and SOCl₂ doped films with and without a PEDOT:PSS layer.

When annealed at 450–500 °C within 3 h in argon, the bilayer performance improved further for an overall decrease in sheet resistances by a factor of 5–7 relative to an undoped, unannealed network. Annealing an analogous CNT network without MoO_x resulted in an enhancement of sheet resistance by a factor of 1.2–1.7. The differences of XPS data for Mo 3*d* and O 1*s* peaks in Mo-O_x-CNT composites before and after thermally activation confirm that the observed effect was due to thermally activated MoO_x-CNT charge transfer interaction.

Stability of the doping effect in the presence of air and water has been questionable. First, especially exposure into the atmosphere is known to substantially degrade the work function of the evaporated films of MoO_x [88]. However, the measurements show the change of sheet resistance to less than 10 % over 20 days in ambient and less than 2% with overnight heating to 300 °C in air. The outstanding stability of the *p*-doping together with high transparency makes the MoO_x-CNT bilayers very promising candidates for CNT electrode formation. Also, MoO_x can be easily deposited either by thermal evaporation or from solution-based precursors [87].

Upon fabrication of transparent electrodes both high electrical conductivity and transparency is important. From this point of view, SWNTs seems to be more suitable for electrode applications than MWNTs. Due to the sparse structure of the CNT network, transparency of 10-100 nm thick films are of the same order for both MWNT and SWNT. However, for the film thicknesses above 100 nm, SWNTs layers are more transparent than MWNTs [89, 90]. For example, 50 nm thick films of SWNT with electrical resistivity of 30 Ω/sq has transmittance >70% in the visible part of the solar spectra and >90% at 2 μm in the near-IR [7]. The latter property presents interest for applications of metallic SWNTs for electrical coupling in photonic devices.

Optical transmittance in the visible spectra is almost the same as that of the commercial ITO. Transmittance vs resistivity plots for SWNT layers show that high aspect ratio of CNTs has an enhanced electrical conductivity in comparison to CNTs with low aspect ratios for the same transparency of CNT thin films. A plausible argument for the enhanced electrical conductivity is that the electrical transport is not fully limited by contact resistances between the CNTs [91]. This effect is clearly observable by transmittance vs resistivity plots for 50 μm and 100 μm long CNTs. Also, breaking of CNTs during the solution preparation via ultrasonic treatment may take place, CNTs with 100 μm length display a lower resistivity of

1.0 k Ω /sq at 30% transmittance. For comparison, electrical resistivity of 50 μ m long CNTs was 1.7 k Ω /sq with the same transmittance of 30%. It is known that individual CNTs tolerate mechanical treatment such as bending, buckling or even certain degree of defect creation without loss of conductivity [92]. The SWNT films prepared [77] from aqueous solutions using surfactants facilitate maximum mechanical flexibility together with solution processability at room temperature also on polymer substrates [77, 93]. CNT coated plastic foil shows the surface resistivity of 100 Ω /m² and transmittance of 97 % as compared with ITO coatings on plastic with the surface resistivity between 5-15 Ω /m² at 72-78 % transmittance [90]. After bending up to 1 mm of the curvature radius, a CNT based device had a performance drop of 20-25 %, which could be restored by a simple heat treatment [93]. Especially for organic photovoltaics, high performance flexible electrodes that can be processed at temperatures <150 °C would support the successful commercialisation of roll-to-roll processed flexible large area solar cells. The doped SWNT thin layers may offer a good alternative for this target, when the conditions for stable doping are technologically adapted.

4.2 CNTs for organic solar cells

With the maximum efficiencies over 5 %, solution-processed bulk heterojunction organic photovoltaic devices using poly-3 hexylthiophene (P3HT) and [6,6]-phenyl-C61-butyric acid methyl ester (PCBM) are the mostly studied material combination for OPVs. Using low band gap polymers as new acceptors in bulk heterojunction solar cells, the OPVs reach efficiencies over 6%. During the last couple of years, the progress was very dynamic, many review papers highlighting the strategic development and reporting new efficiency records were frequently published (see, e.g., Refs. [94, 95]). The developments demonstrate clearly, that OPVS are established as one of the leading next generation photovoltaic

technologies with low cost power production. For the development of CNT electrodes a precise trade-off between its small series resistance and high transparency is targeted. A comprehensive analysis of series resistance (R_s) for highly transparent CNTs films indicated, that the R_s decreases with the film thickness, following an enhanced percolation between the CNTs [96]. Bulk heterojunction devices with P3HT/PCBM deposited by spin coating from o-dichlorobenzene solution as the active layer on ITO and on SWNT electrodes has been studied in Ref. [20]. The photoactive layers were “solvent annealed” overnight and dried at 110 °C for 10 min according to [97]. Thickness of the P3HT/PCBM layer was ~120 nm. Ca (20 nm) and Al (100 nm) were used as counter electrodes. Two methods, vacuum filtering/stamp transferring and ultrasonically spraying were used for SWNT electrode fabrication.

By spray deposition of CMC-dispersed SWNTs, transparent and electrically insulating films of SWNTs can be obtained, which are encapsulated with solid CMC polymer matrix. The electrodes were then soaked in HNO_3 overnight for doping and rinsed in deionized water to wash out the surfactant. After drying, a 100-nm silver busbar pattern was evaporated onto the electrode outside of the active area of the devices. The AFM images in Figs. 3 (a)-(d) display the morphology of the SWNT electrodes. It is important to note that nearly all tubes measured by AFM were single, isolated species. The layers with average height of 1.3 nm are consistent with the expected average diameter for SWNTs. The main difference between the devices using SWNT films ultrasonically sprayed from the CMC dispersion and SWNTs prepared by vacuum filtration was the roughness. The spray coated sample is smooth with an average roughness of few nanometers, where as spikes in a range of 150 nm is characteristic for SWNT thin films prepared by vacuum filtration. Consequently, the shunt resistance, indicative of shorting in the device, is a factor of three lower in the devices prepared by vacuum filtration [Figs. 3 (a)-(d)].

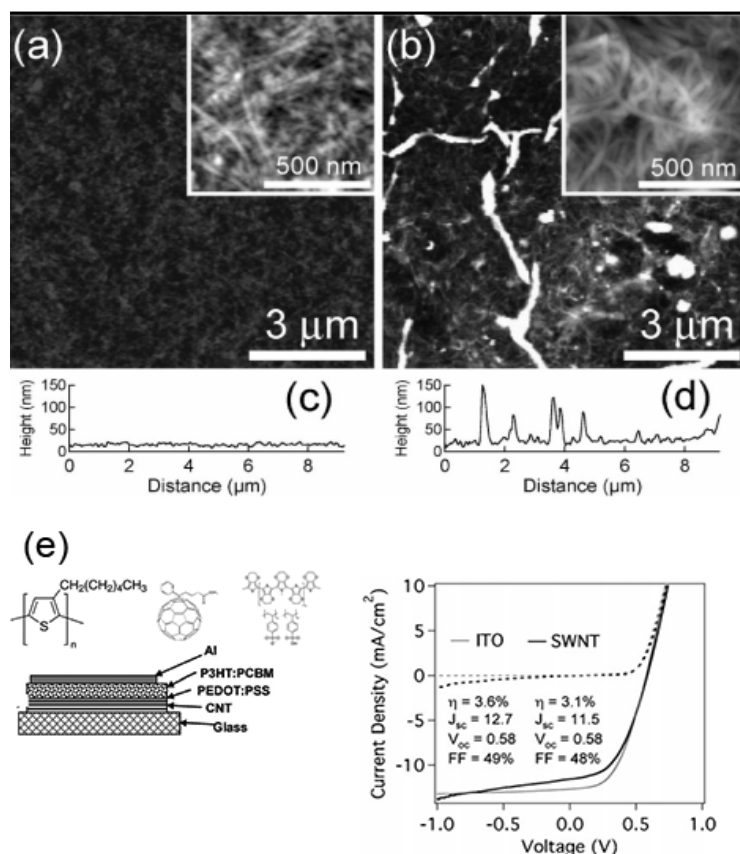


Figure 3. AFM image of transparent SWNT film (a) ultrasonically sprayed from CMC dispersion and treated with HNO_3 . The inset shows the enlarged image of individual SWNTs and/or small bundles. (b) prepared by vacuum filtration and membrane transfer, then treated with HNO_3 . The inset shows the enlarged resolution of larger SWNTs bundles than that observed from the sprayed film. Line scan of (c) sprayed film in panel (a), showing long-range uniformity and low surface roughness as well as of (d) membrane-transferred film in panel (b), demonstrating higher local surface roughness and poor long-range uniformity. (e) Chemical structure of P3HT, PCBM and PEDOT:PSS and the OPV device configuration. Current-voltage dependence for identical P3HT/PCBM devices constructed on transparent SWNT electrode [(- - -) dark curves] ultrasonically sprayed from CMC dispersion or ITO electrode [(—) light curves] displayed on the right side.

Finally, the performance of SWNT layers ultrasonically sprayed from a CMC dispersion was compared to that of ITO in P3HT/PCBM heterojunction solar cells. The only difference between the device structures was that one contained $35 \text{ } \Omega \times \text{sq}^{-1}$ ITO and the other one had $60 \text{ } \Omega \times \text{sq}^{-1}$ SWNT film. Both devices exhibit similar fill factors (FF) of 48 and 49 %, with identical open-circuit voltages (V_{oc}). P3HT/PCBM devices using CNT anodes showed promising solar cell efficiency of 3.1 %, which is somehow smaller than 3.6 % of ITO-based device [Fig. 3e]. An improved solar cell performance has been reported in Ref. [98] with CNT electrode by optimizing the thickness of P3HT/PCBM layer to about 900 nm. The device structures were identical except that one cell was fabricated on $56 \text{ } \Omega \times \text{sq}^{-1}$ ITO whereas the other one was on $60 \text{ } \Omega \times \text{sq}^{-1}$ SWNT film.

Bulk heterojunction solar cells using SWNT/PEDOT:PSS as transparent electrodes displayed the highest efficiency of 4.13 % in this run. In comparison, the same bulk heterojunction device using ITO/PEDOT:PSS as transparent layer had an efficiency of 3.51%. The expected reduction of efficiency occurred because of replacing ITO with SWNT, which is less transparent than ITO. Looking at the effects of hole transport layer (PEDOT:PSS) removal, a tremendous decrease in performance was observed, when PEDOT:PSS was removed from the device on ITO electrode and relatively minimal decrease when it was removed from the device on SWNTs electrodes. The observed cell parameter under AM1.5 illumination are listed in Table III.

Good devices should have high R_{sh} indicating that there are only few parallel parasitic paths for the current transport. R_{sh} drops by two orders of magnitude when SWNTs replace ITO. When PEDOT:PSS is placed on top of glass substrate/SWNT electrode, then the PEDOT:PSS planarizes the SWNT layer and reduces shortening between the the transparent SWNT electrode and counter electrode by physically blocking the parallel paths. R_{sh} does not change significantly when PEDOT:PSS is removed from glass/ ITO-based device. It is

important to figure out that the short circuit current J_{sc} of the cells with both electrodes ITO and SWNTs has been decreased after PEDOT:PSS was removed but, the decrease was much more smaller in case of the SWNT electrodes. Thus, just improvement of morphological control of SWNT electrodes may lead to PEDOT:PSS free bulk heterojunction solar cells with high V_{oc} and efficiencies.

Table III shows the parameters of P3HT&PCBM solar cells with ITO and CNT electrodes. Upon using the spray coating method, the selected surfactant plays a dominant role in determining the solar cell efficiency in the range 1.2-4.1 %. Comparable solar cell performance for the electrodes, prepared from organic solvents and SDS demonstrates, that the methods for the SDS removal without damaging the electrode, are developed successfully. Preparation of CNT electrodes by ultrasonic spray method from CMC dispersion leads to most promising results with efficiencies up to 4.13 %. Dip-coating and filter transferring methods for the preparation of SWNTs without surfactants lead to solar cell efficiencies in the range of 2.2-2.5 %.

TABLE III. *The solar cell parameter of P3HT&PCBM solar cells using ITO and CNT electrodes dependent on the thin film formation method for the CNT electrode. Vacuum filtering technique has been also used for the preparation of the electrodes on flexible polyethylene terephthalate (PET). Solar cell efficiencies are in the same range like the efficiency of spin-casted SWNT layers (3.0 % solar cell efficiency for flexible ITO electrodes and 2.5% for flexible SWNT electrodes using P3HT/PCBM as the active layer).*

Anode	V_{oc} , V	J_{sc} , mA/cm ²	FF	PCE	Method
<i>Glass /ITO [86] /PEDOT:PSS</i>	<i>0.55</i>	<i>8.4</i>	<i>50.0</i>	<i>2.3</i>	<i>Reference</i>
<i>Glass/SWNT/PEDOT:PSS[86]</i>	<i>0.55</i>	<i>9.9</i>	<i>43.1</i>	<i>2.3</i>	<i>Spray coating</i>
<i>Glass/SWNT/PEDOT:PSS[86]</i>	<i>0.55</i>	<i>6.7</i>	<i>31.4</i>	<i>1.2</i>	<i>Spray coating</i>
<i>Glass/SWNT/PEDOT:PSS[86]</i>	<i>0.59</i>	<i>7.3</i>	<i>46.4</i>	<i>2.2</i>	<i>Spray coating</i>
<i>Glass/SWNT/PEDOT:PSS[86]</i>				<i>2.3</i>	<i>Spin coating</i>

Glass / ITO [20]	0.48	7.42	40.6	1.44	Reference
Glass/ITO/PEDOT:PSS [20]	0.59	10.8	55.3	3.5	Ultrasonic Spray
Glass / SWNT [20]	0.54	11.39	55.4	3.37	Ultrasonic Spray
Glass/SWNT/PEDOT:PSS [99]	0.57	13.78	52.9	4.13	Ultrasonic Spray
Glass/SWNT/PEDOT:PSS [100]		8.1	50.0	2.3	Dip casting of ZnO coated steel fiber
Glass/MWNT PEDOT:PSS [101]	0.49	5.47	0.49	1.3	Vertically growth via CVD
PET/ITO/PEDOT:PSS [93]	0.61	8.6	61	3.0	Reference
PET/SWNT/Glass/PEDOT:PSS [93]	0.61	7.8	52	2.5	Vacuum Filtering/ PDMS Stamp Transferring

Beside CNTs, the recently reported alternatives of transparent electrodes include poly (3,4-ethylenedioxythiophene): poly(styrenesulfonate) (PEDOT:PSS) with metal grids [102], graphene [103] and silver nanowires [104, 105]. All these alternatives can be fabricated via ink-jet printing, screen printing, slot-die coating, or similar solution based processes on glass or on flexible PET substrates. The best parameters of the alternative electrodes in terms of sheet resistance and transparency on flexible substrates are compared in Table IV.

TABLE IV. Flexible electrodes for organic solar cells and their characteristics.

Electrode	Sheet Resistance [Ohm/sq]	Transparency [%]
Sputtered ITO on PET [106]	60	79
PEDOT:PSS [107]	63	67
PEDOT:PSS and metal grid combination [102]	1	92
CNTs [65]	40	70
Graphene [108]	30	90

All these alternatives have the risk to alter device performance via changes to the series resistance across the device, lower transparency leading to lower photogenerated current and effects on the lifetime. However, such effects could be tolerated if the overall cost or energy requirements for manufacturing of OPV modules were significantly reduced. PEDOT:PSS with metal grid combination is the most promising candidate with the highest

transparency and the lowest sheet resistance to replace ITO electrode. We can say that only if the cost of CNTs drops significantly, by avoiding the material lost via developing selective CNT synthesis methods, CNTs can become competitive as an alternative to ITO.

4.3 Semiconducting CNTs as a part of active layer

Role of *p*-SWNTs as charge separation and selective hole collection layer has also been investigated in OPVs. In one of the first such studies [109], SWCNT was blended with poly(3-octylthiophene) (P3OT) to fabricate bulk heterojunction solar cells. It was claimed that there are mainly two effects of SWNTs in the OPV. First, SWNTs facilitate exciton dissociation at the interface between the *p*-type polymer, P3OT and SWCNTs; second, SWNTs provide a ballistic pathway for the charge carrier to transport. However, the power conversion efficiency of P3OT/SWCNT bulk heterojunction solar cells was very low (<0.1%), because there was not enough interface area between P3OT and SWCNTs to sufficiently dissociate excitons due to the insolubility of SWNTs in organic solvents. The concentration of SWNTs in photo active layer was lower than 1%. To tackle this problem, SWNTs were functionalized on their side walls to enhance the solubility and then used to fabricate homogeneous bulk heterojunction devices with a high concentration of SWNTs [110]. But also there, not a noticeable improvement has been reported, probably due to the increased carrier recombination at the functionalized CNTs.

Poly(3-hexylthiophene) (P3HT) and 1-(3-methoxycarbonyl)propyl-1-phenyl[6,6] C₆₁ (PCBM) are, to date, the most-studied active materials around the world for the organic bulk-heterojunction structure. For a typical organic solar cell in bulk heterojunction configuration (1:1-P3HT:PCBM blends), the electron mobility in the PCBM phase is about 1 order of magnitude higher than that of holes in P3HT phase after annealing at 120°C [94, 111].

Similarly, for polymer/SWNT blends to show any promise for OPV, it is very important to demonstrate that excitons are dissociated by charge transfer at the polymer/CNT heterojunction interface. Some analysis in the literature clearly demonstrated the evidence, that electron transfer from p-type P3HT on SWNT occurs but a hole transfer from SWNT onto the P3HT does not occur [112]. Facts to verify this thesis is modulation of properties of P3HT by a) quenching of photoluminescence by nearly 90 % by incorporating small amounts of SWNTs, b) 100 fold-enhancement of photoconductance signal for 532 nm excitation by time-resolved microwave conductivity measurements, and c) enhancement of charge carrier lifetime compared to neat P3HT [112].

Although an improvement in solar cell parameters have been reported in some research groups using CNTs in P3HT/PCBM blends, it has been also observed that the profitable concentration range of the CNTs in bulk heterojunction blend is strongly limited. Increasing the thickness of the P3HT/PCBM solar cells using CNTs has been realized successfully. On the other hand, P3HT:PCBM-based active layer of about 100-200 nm can absorb most part of the sunlight. So, further increasing the thickness beyond 250 nm had only little impact on improving the cell efficiency.

One of the limiting factor for the efficiency enhancement is that the organic solar cell morphology strongly influences on solar cell efficiency. Due to the compatible transport properties of donor/acceptor pair P3HT/PCBM, the fill factor 70 % of pure organic solar cells can be said as satisfactory for OPVs. While nanotubes are able to deliver dissociated charge carriers to the electrode at high speed, the nanomorphology of polymer/fullerene mixture might be changed above a critical concentration of CNTs, limiting the solar cell performance. Additionally, coexistence of metallic and semiconducting nanotubes in the photo active area might enhance the charge carrier recombination rate. Although only 1/3 of the SWNTs is metallic, its detrimental effect on photo active layer of organic solar cells with usual thickness

of 100-150 nm is not negligible. Considering the presence of metallic SWNTs, electrons in LUMO of PCBM and holes in HOMO of P3HT can recombine in metallic SWNTs.

SWNTs dispersed in dichloroethane were used [113] as hole transport layer in bilayer configuration of the cells. Insertion of a 12.2 nm thick SWNTs between the P3HT/PCBM bulk heterojunction and transparent electrode resulted in power conversion efficiency 3.04 %, which is larger than 1.16 % and 2.84 % for the P3HT/PCBM devices without and with the traditional PEDOT:PSS as the HTL, respectively [113]. Finally, despite the encouraging spectroscopic results on electron transfer, blending SWNT in organic heterojunction blend have not strong effect on the solar cell performance improvement [112, 114]. Currently, researchers shifted their focus clearly from OPVs to organic/inorganic hybrid solar cells investigating CNTs in combination with classical inorganic solar cell materials.

4.4 CNTs for Si-based solar cells

Capability of good light absorbance and very low reflective properties of CNT were used also to construct Si wafer-based heterojunction solar cells, where CNTs play multiple roles, including charge separation, charge transport and light harvesting. The first CNT-Si heterojunction cells configuration Ag/CNT/*n*-Si/Ti/Pd/Ag with 1.3 % efficiency were prepared in Ref. [115]. The cells were fabricated by coating of a transparent double walled CNT (DWNTs) film of 50 nm thickness on *n*-Si of thickness of 525 nm. The DWNTs had an outer diameter of 2.0-2.5 nm and usually were arranged in 20-50 nm diameter bundles according the HRTEM characterization. DWNT films of thicknesses of 35-55 nm show a transmission of >60% in the visible light region to ensure the light absorption on *n*-Si wafer. DWNT film were consisting of metallic as well as semiconducting CNTs. Nevertheless, the device showed a high rectification ratio in the dark and an open circuit voltage of 0.5 V,

short-circuit current density of 13.8 mA/cm^2 under AM1.5 illumination with an intensity of 100 mW/cm^2 . This indicates to formation of p/n heterojunctions between the DWNTs and n -Si that favors charge separation as well as electron and hole transfer through n -Si and CNTs, respectively.

Similarly, SWNT/ n -Si solar cells were prepared [116] forming SWNT thin layers on n -Si using spray coating method. The SWNT diameter was 0.6-1.1 nm whereas the thickness of the SWNT bundles was around 20 nm. SWNT films of thickness of 50 nm had an transmittance of 69 % at 550 nm. Under AM1.5 illumination, an open circuit voltage of 0.45 V and short-circuit current density of 15.0 mA/cm^2 were measured. Because of the poor fill-factor of 28 %, the solar cell efficiency was 0.95 %. By adding three droplets of pure SOCl_2 - a strong oxidizing agent- followed by drying in the air, an enhancement of photo current to 21.0 mA/cm^2 was reported. All the other solar cell parameters remained constant. Hall effect measurements displayed charge mobilities of 0.23 and $1.02 \text{ cm}^2 \text{ V}^{-1}\text{s}^{-1}$ for SWNTs and SOCl_2 -SWNT films. Electron-withdrawing ability of SOCl_2 , when adsorbed on the CNT surface, can enable an increase in the density of states near the Fermi level in SWNT by shifting it into the van Hove singularity region [117]. NT on silicon (Si) heterojunction solar cells with efficiencies above 7% is reported in Ref. [118]. The cells consist of an n -Si wafer coated by a spiderweb-like thin film of double-walled CNTs (DWNTs) through a solution transfer process on water. The solar cell configuration was Ag/DWNT/ n -Si/Au/Ti [Fig. 4], which showed open circuit voltage 0.54 V, short circuit current density 26 mA/cm^2 , fill factor 53%, and a conversion efficiency 7.4%.

Alternative to the p/n junction-modell, a metal–semiconductor (MS) Schottky barrier junction between the metallic DWNTs and n -Si was discussed in Ref. [118]. The device structures fabricated by replacing DWNTs by MWNTs, which are also metallic, exhibited almost the same open circuit voltage $V_{oc} = 0.5 \text{ V}$ as that of DWNTs, but about 30 times

smaller short current density $J_{sc}=0.8 \text{ mA cm}^{-2}$. In the cells, the diffusion barrier formed because of the Fermi level equilibration in the n -Si/CNT junction initiates electron transfer from n -Si to the metallic CNT, generates a depletion layer and band bending in Si in the close vicinity of nanotubes. The photons absorbed in Si generate electron/hole pairs that will be separated by the built-in potential enabling photovoltaic power generation. The Schottky junction formed at the interface between metallic CNT and n - Si lead to solar cell efficiencies about two orders of magnitude lower than DWNT-Si cells indicating the necessity of p/n junction for higher solar cell efficiencies in this material combination [118].

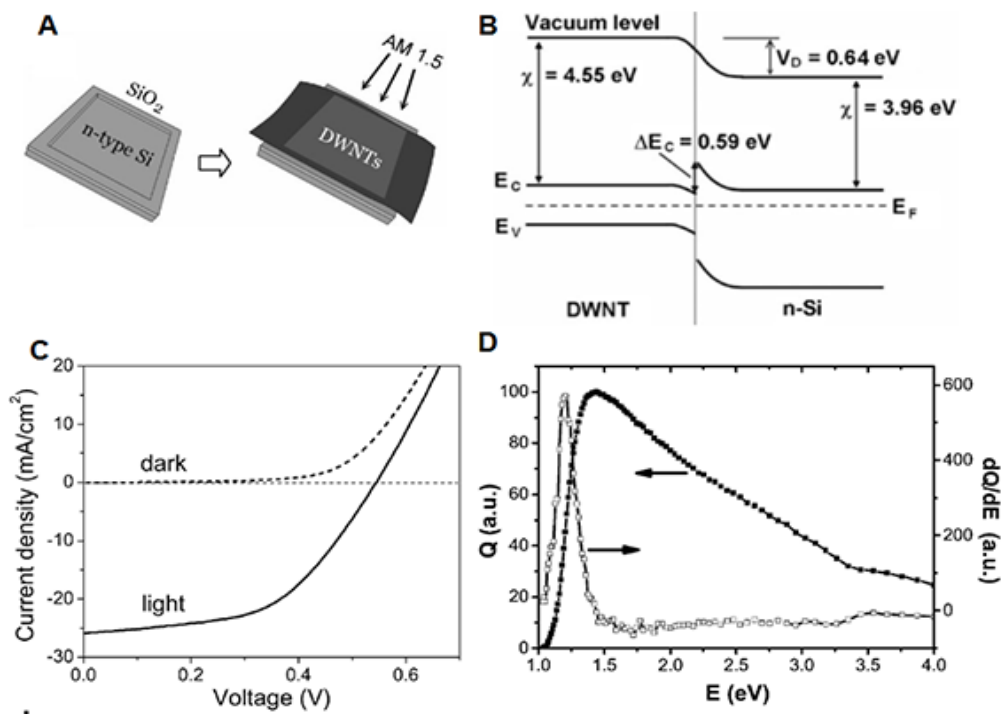


Figure 4. (From Ref. [118]) (A) DWNT-Si heterojunctions. (B) Band scheme diagram of the DWNT-Si heterojunction. (C) Dark and light J - V curves of a p -DWNT/Si heterojunction cell, showing a V_{oc} of 0.54 V, a J_{sc} of 26 mA cm^{-2} , a fill factor of 53%, and an efficiency of 7.4%. (D) Plots of the quantum efficiency (Q) and its derivative against photon energy E measured from a DWNT-Si cell.

The cell efficiency of 6% has been reported in Ref. [119] by using a mixture of SWNTs and DWNTs with diameters in the range of 0.3-3 nm deposited on *n*-Si. Efficiency of the cells has been increased to 10% by H₂O₂ treatment. The I-V characteristics displayed $J_{sc}=29.3 \text{ mA/cm}^2$, $V_{oc}=0.55 \text{ V}$ and $FF=64.4\%$ for the H₂O₂- post-treated cells. According to X-ray photoelectron spectra (XPS) of *n*-Si/*p*-CNTs, H₂O₂- treatment surprisingly positively affects the Si surface but not on the CNT bundles. The hypothesis about the mechanism of the solar cell efficiency enhancement is related to the redox reaction between H₂O₂ and Si surface forming numerous CNT-Si-H₂O₂ photoelectrochemical cells (PEC) and CNT-Si heterojunction cells. In the PEC, H₂O₂ is reduced to H₂O and Si is oxidized to SiO₂. The redox reaction generates free charges, which reduce the series resistance and enhance the photo-induced current. CNTs act as inner counter electrode in the PEC. In the metal-insulator-semiconductor (MIS) Schottky structure formed by insertion of a few nanometer thin SiO_x insulator between the Si and metal, minority charge carriers will be transported through the insulating layer by CNT fibers [119]. By applying a series of doping and gating methods such as SOCl₂ treatment [116], ionic liquid electrolyte infiltration and electronic gating [120, 121] as well as nitric acid doping [122], the power conversion efficiencies of the CNT-Si cells have been continuously pushed from initially about 1.3% to 13.8% (within the last several years).

The environmental stability of the DWNT-Si solar cells has been tested in air for a prolonged time within up to 400 h (Ref. [118]). V_{oc} and J_{sc} remained constant. Also, in these experiments, CNT thin film was formed using a mixture of metallic and semiconducting CNT bundles [118]. To test the mechanical robustness, solar cells using mixtures of DWNTs and SWNTs on flexible monocrystalline Si thin films are fabricated. The CNT/Si thin-film cells have shown initial efficiencies of approximately 3% to 5% depending on the thickness of Si wafer (5 to 50 μm) and reaches 6% by HNO₃ doping. The CNT/Si thin-film cells have

shown a good stability in bending-recovery cycles. For the ultrathin Si films with a thickness less than 20 μm , the maximum bending angle could exceed 50° [123].

In recent years, the studies are focussed on the development of multifunctional CNT thin films, p/n junction formation together with advanced light trapping effects. A remarkably high fill factor of 72 % is achieved [124] in SWNTs with self assembled hierarchical microhoneycomb network structure ($\mu\text{-HN}$) on $n\text{-Si}$. The hierarchical $\mu\text{-HN}$ consists of dense walls and a bucky paper bottom, which simultaneously increases the optical transmittance and decreases the sheet resistance. The I-V characteristics displayed $J_{\text{sc}}=15.9 \text{ mA/cm}^2$, $V_{\text{oc}}=0.53 \text{ V}$, and efficiency exceeding 10 % obtained in the dry state after treatment with dilute nitric acid. The solar cells from intrinsic $p\text{-SWNT}$ thin-films deposited on $n\text{-Si}$ wafers exhibited device ideality factor close to unity and a record-high power-conversion-efficiency of $>11\%$ without high-temperature processing for $p\text{-}n$ junction formation.

Combination of CNTs, graphene or conducting polymers with conventional Si wafers has led to developing of advanced solar cell architectures. CNT-Si junction 15 mm^2 area solar cells with efficiencies reaching 15% is reported in Ref. [125]. Such high efficiency has been achieved by coating a TiO_2 antireflection layer and doping CNTs with oxidative chemicals under AM 1.5 illumination. By using metal oxides as antireflection layer, further increased the photocurrent and solar cell efficiency up to 17% [19] in $p\text{-SWNT}/n\text{-Si}$ and $n\text{-SWNT}/p\text{-Si}$ heterojunction solar cells using MoO_x and ZnO .

5. Conclusion

Replacing the transparent indium tin oxide electrode by CNT spiderwebs have displayed comparable solar cell efficiencies in organic solar cells together with improved mechanical flexibility. The reversibility of the doping process is still a challenge for the organic solar cells limiting the long time stability and the operation temperature. To solve this problem, alternative methods for a strong and irreversible p-doping process using MoO_x have

been introduced recently. The p/n junctions in organic solar cells suffer generally by polydispersive electrical properties of CNTs because the evidence of metallic CNTs enhances the number of recombination centers. On the other hand, p-SWNTs in combination with n-Si illustrate important future research directions for CNTs promising results of academic interest for organic/inorganic hybrid solar cells. By increasing the optical transmittance and simultaneously decreasing the sheet resistance, *p*-CNT/*n*-Si solar cells have brought solar power conversion efficiencies 17%. We suggest that one of the important research direction should be the critical evaluation of photovoltaic device parameter as a function of SWNT diameter for primary p-type SWNTs with well-defined electrical properties. One may ask what is the argument for adding CNTs to Si solar cells that already exhibit efficiencies above 24%. Clearly, the knowledge gained in this studies can be transfered to new types of nanostructured hybrid solar cell structures with extended absorption properties in near IR regime using CNTs and inorganic semiconducting nanocrystals. In summary, there is a great progress in understanding and optimizing the operational stability of CNTs as transparent electrodes in organic solar cells and as photo-active materials in organic/inorganic hybrid solar cells.

Acknowledgements. This work is supported by the Scientific and Technological Research Council of Turkey (TÜBİTAK)- BİDEP 2232-Program and New Indigo ERA.NET project 237643/E20.

References

- 1 C. G. Granqvist. *Sol. Energy Mater. Sol. Cells.* (2007), **91**(17), 1529-98.
- 2 P. Barquinha, R. Martins, L. Pereira, et al. *Transparent Semiconductors: From Materials to Devices.* : West Sussex: Wiley & Sons 2012.
- 3 K. S. Novoselov, A. K. Geim, S. V. Morozov, et al. *Science.* (2004), **306**(5696), 666-9.
- 4 A. K. Geim, K. S. Novoselov. *Nat Mater.* (2007), **6**(3), 183-91.
- 5 J. K. Wassei, R. B. Kaner. *Materials Today.* (2010), **13**(3), 52-9.
- 6 L. Chen, H. He, H. Yu, et al. *Electrochimica Acta.* (2014), **130**(0), 279-85.
- 7 Z. Wu, Z. Chen, X. Du, et al. *Science.* (2004), **305**(5688), 1273-6.
- 8 S. Dresselhaus, G. Dresselhaus, P. Avouris. *Carbon Nanotubes: Synthesis, Structure, Properties, and Applications:* Springer; 2001.
- 9 P. Blake, P. D. Brimicombe, R. R. Nair, et al. *Nano Lett.* (2008), **8**(6), 1704-8.
- 10 K. Novoselov, L. BRITNELL. *Photovoltaic cells.* US Patent Application PCT/GB2013/050753, 2013.
- 11 T. J. Echtermeyer, L. Britnell, P. K. Jasnós, et al. *Nat Commun.* (2011), **2**, 458.
- 12 X. Wang, L. Zhi, K. Mullen. *Nano Lett.* (2007), **8**(1), 323-7.
- 13 Q. Liu, Z. Liu, X. Zhang, et al. *Appl. Phys. Lett.* (2008), **92**(22), 223303-3.
- 14 Y. Xu, G. Long, L. Huang, et al. *Carbon.* (2010), **48**(11), 3308-11.
- 15 X. Li, H. Zhu, K. Wang, et al. *Adv. Mater.* (2010), **22**(25), 2743-8.
- 16 R. Won. *Nat Photon.* (2010), **4**(7), 411-.
- 17 S. Z. Karazhanov, F. Ait Medjane, J. Zhu, et al. 26th EU PVSEC; Hamburg, Germany 2011.
- 18 S. Z. Karazhanov, M. Nawaz. *Thin film solar cell electrode with graphene electrode layer.* US Patent Application WO 2011NO00127 20110415, 2011.
- 19 F. Wang, D. Kozawa, Y. Miyauchi, et al. *Nat Commun.* (2015), **6**.

- 20 R. C. Tenent, T. M. Barnes, J. D. Bergeson, et al. *Adv. Mater.* (2009), **21**(31), 3210-6.
- 21 R. Saito, M. Fujita, G. Dresselhaus, et al. *Appl. Phys. Lett.* (1992), **60**(18), 2204-6.
- 22 K. Yanagi, Y. Miyata, T. Tanaka, et al. *Diamond Relat. Mater.* (2009), **18**(5–8), 935-9.
- 23 R. Xiang, E. Einarsson, Y. Murakami, et al. *ACS Nano.* (2012), **6**(8), 7472-9.
- 24 Z. Li, V. Kunets, V. Saini, et al. *ACS Nano.* (2009), **3**, 1407 - 14.
- 25 M. A. Bissett, J. G. Shapter. *J. Phys. Chem. C.* (2010), **114**(14), 6778-83.
- 26 S. Barazzouk, S. Hotchandani, K. Vinodgopal, et al. *J. Phys. Chem. B.* (2004), **108**(44), 17015-8.
- 27 M. A. El Khakani, V. Le Borgne, B. Aïssa, et al. *Appl. Phys. Lett.* (2009), **95**(8), 083114.
- 28 P.-X. Hou, C. Liu, H.-M. Cheng. *Carbon.* (2008), **46**(15), 2003-25.
- 29 A. Rao, E. Richter, S. Bandow, et al. *Science.* (1997), **275**(5297), 187-91.
- 30 X. Zhao, Y. Ando, L. C. Qin, et al. *Phys. B.* (2002), **323**(1–4), 265-6.
- 31 T. W. Ebbesen, P. M. Ajayan. *Nature.* (1992), **358**(6383), 220-2.
- 32 N. Grobert. *Mater. Today.* (2007), **10**(1–2), 28-35.
- 33 A. M. Morales, C. M. Lieber. *Science.* (1998), **279**(5348), 208-11.
- 34 P. G. Collins, K. Bradley, M. Ishigami, et al. *Science.* (2000), **287**, 1801.
- 35 A. C. Dillon, P. A. Parilla, J. L. Alleman, et al. *Chem. Phys. Lett.* (2005), **401**(4–6), 522-8.
- 36 J. Kong, A. M. Cassell, H. Dai. *Chem. Phys. Lett.* (1998), **292**(4–6), 567-74.
- 37 E. Mayhew, V. Prakash. *Carbon.* (2013), **62**(0), 493-500.
- 38 Y. Murakami, Y. Miyauchi, S. Chiashi, et al. *Chem. Phys. Lett.* (2003), **374**(1–2), 53-8.
- 39 H. Hu, P. Bhowmik, B. Zhao, et al. *Chem. Phys. Lett.* (2001), **345**(1–2), 25-8.
- 40 L. A. Montoro, J. M. Rosolen. *Carbon.* (2006), **44**(15), 3293-301.
- 41 S. M. Bachilo, L. Balzano, J. E. Herrera, et al. *J. Am. Chem. Soc.* (2003), **125**(37), 11186-7.

- 42 S. Lee, C. Zoican Loebick, L. D. Pfefferle, et al. *J. Phys. Chem. C.* (2011), **115**(4), 1014-24.
- 43 E. Dervishi, Z. Li, F. Watanabe, et al. *J. Mater. Chem.* (2009), **19**(19), 3004-12.
- 44 Y. Miyauchi, S. Chiashi, Y. Murakami, et al. *Chem. Phys. Lett.* (2004), **387**(1-3), 198-203.
- 45 T. Thurakitserree, C. Kramberger, P. Zhao, et al. *Carbon.* (2012), **50**(7), 2635-40.
- 46 S. Sakurai, M. Inaguma, D. Futaba, et al. *Materials.* (2013), **6**(7), 2633-41.
- 47 T. Tanaka, Y. Urabe, D. Nishide, et al. *J. Am. Chem. Soc.* (2011), **133**(44), 17610-3.
- 48 G. Hong, B. Zhang, B. Peng, et al. *J. Am. Chem. Soc.* (2009), **131**(41), 14642-3.
- 49 L. Zhang, X. Tu, K. Welsher, et al. *J. Am. Chem. Soc.* (2009), **131**(7), 2454-5.
- 50 T. Palacin, H. L. Khanh, B. Jusselme, et al. *J. Am. Chem. Soc.* (2009), **131**(42), 15394-402.
- 51 L. Zhang, S. Zaric, X. Tu, et al. *J. Am. Chem. Soc.* (2008), **130**(8), 2686-91.
- 52 H.-M. So, B.-K. Kim, D.-W. Park, et al. *J. Am. Chem. Soc.* (2007), **129**(16), 4866-7.
- 53 J. L. Bahr, E. T. Mickelson, M. J. Bronikowski, et al. *Chem. Commun.* (2001), (2), 193-4.
- 54 K. K. Kim, D. J. Bae, C.-M. Yang, et al. *J. Nanosci. Nanotechnol.* (2005), **5**(7), 1055-9.
- 55 S. D. Bergin, Z. Sun, D. Rickard, et al. *ACS Nano.* (2009), **3**(8), 2340-50.
- 56 S. D. Bergin, Z. Sun, P. Streich, et al. *J. Phys. Chem. C.* (2010), **114**(1), 231-7.
- 57 S. D. Bergin, V. Nicolosi, P. V. Streich, et al. *Adv. Mater.* (2008), **20**(10), 1876-81.
- 58 J. Lyklema. *Colloids Surf. A.* (1999), **156**(1-3), 413-21.
- 59 H. Kataura, Y. Kumazawa, Y. Maniwa, et al. *Synth. Met.* (1999), **103**(1-3), 2555-8.
- 60 M. L. Usrey, A. Chaffee, E. S. Jeng, et al. *J. Phys. Chem. C.* (2009), **113**(22), 9532-40.
- 61 Y. Kim, D. Lee, Y. Oh, et al. *Synth. Met.* (2006), **156**(16-17), 999-1003.
- 62 K. Balasubramanian, M. Burghard. *Small.* (2005), **1**(2), 180-92.

- 63 S. Kim, J. Yim, X. Wang, et al. *Adv. Funct. Mater.* (2010), **20**(14), 2310-6.
- 64 C. L. Kane, E. J. Mele. *Phys. Rev. Lett.* (1997), **78**(10), 1932-5.
- 65 H.-Z. Geng, K. K. Kim, K. P. So, et al. *J. Am. Chem. Soc.* (2007), **129**(25), 7758-9.
- 66 M. Shimizu, S. Fujii, T. Tanaka, et al. *J. Phys. Chem. C.* (2013), **117**(22), 11744-9.
- 67 G. S. Duesberg, A. P. Graham, M. Liebau, et al. *Nano Lett.* (2003), **3**(2), 257-9.
- 68 Y. T. Lee, N. S. Kim, J. Park, et al. *Chem. Phys. Lett.* (2003), **372**(5-6), 853-9.
- 69 B. Wang, C. H. P. Poa, L. Wei, et al. *J. Am. Chem. Soc.* (2007), **129**(29), 9014-9.
- 70 B. B. Wang, S. Lee, X. Z. Xu, et al. *Appl. Surf. Sci.* (2004), **236**(1-4), 6-12.
- 71 W. Z. Li, S. S. Xie, L. X. Qian, et al. *Science.* (1996), **274**(5293), 1701-3.
- 72 M. Terrones, N. Grobert, J. Olivares, et al. *Nature.* (1997), **388**(6637), 52-5.
- 73 Z. F. Ren, Z. P. Huang, J. W. Xu, et al. *Science.* (1998), **282**(5391), 1105-7.
- 74 H. Anwar, A. E. George, I. G. Hill. *Solar Energy.* (2013), **88**(0), 129-36.
- 75 H. Borchert, F. Witt, A. Chanaewa, et al. *J. Phys. Chem. C.* (2012), **116**(1), 412-9.
- 76 S. Huang, L. Dai, A. W. H. Mau. *J. Phys. Chem. B.* (1999), **103**(21), 4223-7.
- 77 B. B. Parekh, G. Fanchini, G. Eda, et al. *Appl. Phys. Lett.* (2007), **90**(12), 121913.
- 78 W. Bauhofer, J. Z. Kovacs. *Compos. Sci. Technol.* (2009), **69**(10), 1486-98.
- 79 Q. Cao, J. A. Rogers. *Adv. Mater.* (2009), **21**(1), 29-53.
- 80 D. Zhang, K. Ryu, X. Liu, et al. *Nano Lett.* (2006), **6**(9), 1880-6.
- 81 R. B. Weisman, S. M. Bachilo. *Nano Lett.* (2003), **3**(9), 1235-8.
- 82 J. W. G. Wilder, L. C. Venema, A. G. Rinzler, et al. *Nature.* (1998), **391**(6662), 59-62.
- 83 R. Jackson, B. Domercq, R. Jain, et al. *Adv. Funct. Mater.* (2008), **18**(17), 2548-54.
- 84 F. Hennrich, R. Wellmann, S. Malik, et al. *Phys. Chem. Chem. Phys.* (2003), **5**(1), 178-83.
- 85 H. Gao, R. Izquierdo, V.-V. Truong. *Chem. Phys. Lett.* (2012), **546**(0), 109-14.
- 86 Y. Jung, X. Li, N. K. Rajan, et al. *Nano Lett.* (2013), **13**(1), 95-9.

- 87 S. L. Hellstrom, M. Vosgueritchian, R. M. Stoltenberg, et al. *Nano Lett.* (2012), **12**(7), 3574-80.
- 88 Irfan, H. Ding, Y. Gao, et al. *Appl. Phys. Lett.* (2010), **96**(24), 243307.
- 89 R. M. Jain, R. Howden, K. Tvrdy, et al. *Adv. Mater.* (2012), **24**(32), 4436-9.
- 90 M. Kaempgen, G. S. Duesberg, S. Roth. *Appl. Surf. Sci.* (2005), **252**(2), 425-9.
- 91 M. Shiraishi, M. Ata. *Synth. Met.* (2002), **128**(3), 235-9.
- 92 A. Hirsch. *Angew. Chem. Int. Ed.* (2002), **41**(11), 1853-9.
- 93 M. W. Rowell, M. A. Topinka, M. D. McGehee, et al. *Appl. Phys. Lett.* (2006), **88**(23), 233506.
- 94 C. J. Brabec, S. Gowrisanker, J. J. M. Halls, et al. *Adv. Mater.* (2010), **22**(34), 3839-56.
- 95 M. C. Scharber, N. S. Sariciftci. *Prog. Polym. Sci.* (2013), **38**(12), 1929-40.
- 96 L. Hu, D. S. Hecht, G. Grüner. *Nano Lett.* (2004), **4**(12), 2513-7.
- 97 G. Li, Y. Yao, H. Yang, et al. *Adv. Funct. Mater.* (2007), **17**(10), 1636-44.
- 98 T. M. Barnes, J. D. Bergeson, R. C. Tenent, et al. *Appl. Phys. Lett.* (2010), **96**(24), 243309.
- 99 T. M. Barnes, X. Wu, J. Zhou, et al. *Appl. Phys. Lett.* (2007), **90**(24), 243503-3.
- 100 D. Liu, M. Zhao, Y. Li, et al. *ACS Nano.* (2012), **6**(12), 11027-34.
- 101 R. Ulbricht, S. B. Lee, X. Jiang, et al. *Sol. Energy Mater. Sol. Cells.* (2007), **91**(5), 416-9.
- 102 Y. Galagan, J.-E. J.M. Rubingh, R. Andriessen, et al. *Sol. Energy Mater. Sol. Cells.* (2011), **95**(5), 1339-43.
- 103 K. C. Kwon, W. J. Dong, G. H. Jung, et al. *Sol. Energy Mater. Sol. Cells.* (2013), **109**(0), 148-54.
- 104 D.-S. Leem, A. Edwards, M. Faist, et al. *Adv. Mater.* (2011), **23**(38), 4371-5.
- 105 Z. Yu, L. Li, Q. Zhang, et al. *Adv. Mater.* (2011), **23**(38), 4453-7.

- 106 Sigma-Aldrich. www.sigmaaldrich.com. 2014;
- 107 S.-I. Na, B.-K. Yu, S.-S. Kim, et al. *Sol. Energy Mater. Sol. Cells*. (2010), **94**(8), 1333-7.
- 108 S. Bae, H. Kim, Y. Lee, et al. *Nat. Nanotechnol.* (2010), **5**(8), 574-8.
- 109 E. Kymakis, G. A. J. Amaratunga. *Appl. Phys. Lett.* (2002), **80**(1), 112-4.
- 110 B. Pradhan, S. K. Batabyal, A. J. Pal. *Appl. Phys. Lett.* (2006), **88**(9), 093106.
- 111 L. Liu, W. E. Stanchina, G. Li. *Appl. Phys. Lett.* (2009), **94**(23), 233309.
- 112 A. J. Ferguson, J. L. Blackburn, N. Kopidakis. *Materials Letters*. (2013), **90**, 115-25.
- 113 E. Kymakis, M. M. Stylianakis, G. D. Spyropoulos, et al. *Sol. Energy Mater. Sol. Cells*. (2012), **96**(0), 298-301.
- 114 S. Berson, R. de Bettignies, S. Bailly, et al. *Adv. Funct. Mater.* (2007), **17**(16), 3363-70.
- 115 J. Wei, Y. Jia, Q. Shu, et al. *Nano Lett.* (2007), **7**, 2317 - 21.
- 116 Z. Li, V. Kunets, V. Saini, et al. *Appl Phys Lett.* (2008), **93**, 243117.
- 117 U. Dettlaff-Weglikowska, V. Skákalová, R. Graupner, et al. *Journal of the American Chemical Society*. (2005), **127**(14), 5125-31.
- 118 Y. Jia, J. Wei, K. Wang, et al. *Adv Mater.* (2008), **20**, 4594 - 8.
- 119 X. Bai, H. Wang, J. Wei, et al. *Chem. Phys. Lett.* (2012), **533**(0), 70-3.
- 120 P. Wadhwa, B. Liu, M. A. McCarthy, et al. *Nano Lett.* (2010), **10**(12), 5001-5.
- 121 P. Wadhwa, G. Seol, M. K. Petterson, et al. *Nano Lett.* (2011), **11**(6), 2419-23.
- 122 Y. Jia, A. Cao, X. Bai, et al. *Nano Lett.* (2011), **11**, 1901 - 5.
- 123 H. Sun, J. Wei, Y. Jia, et al. *Nanoscale Res. Lett.* (2014), **9**(1), 514.
- 124 K. Cui, T. Chiba, S. Omiya, et al. *J. Phys. Chem. Lett.* (2013), **4**(15), 2571-6.
- 125 E. Shi, L. Zhang, Z. Li, et al. *Sci. Rep.* (2012), **2**.

